Available online at www.sciencedirect.com

ScienceDirect

materialstoday: PROCEEDINGS

Materials Today: Proceedings 1S (2014) 193 – 208

Absence of circular polarisation in reflections of butterfly wing scales with chiral Gyroid structure

Matthias Saba[a,*], Bodo D. Wilts[b,c,*], Johannes Hielscher[a], Gerd E. Schröder-Turk[a,d,**]

[a] *Institut für Theoretische Physik, Friedrich-Alexander Universität Erlangen-Nürnberg, Erlangen, Germany*
[b] *Computational Physics, Zernike Institute for Advanced Materials, University of Groningen, Groningen, the Netherlands*
[c] *Cavendish Laboratory, Department of Physics, University of Cambridge, J.J. Thomson Avenue, Cambridge, UK*
[d] *Applied Maths, Research School of Physical Sciences and Engineering, The Australian National University, Canberra, Australia*

Abstract

The *single Gyroid*, a triply-periodic ordered chiral network of cubic symmetry, appears as a nanostructure in the green-colored wing scales of various butterflies. In lossless and perfectly ordered single Gyroid materials, the structural chirality leads to circularly polarized reflections from crystals oriented in the [100] direction. Here we report a circular polarisation study of the macroscopic reflections of the wing scales of *Callophrys rubi* and *Teinopalpus imperialis* that reveals no circular dichroism, that is, we find no significant difference in the reflectance values for left- and right-circularly polarized light. The reasons for the absence of circularly polarized reflections is likely to be a compound effect of various factors, including crystallite orientation, presence of both left- and right-handed single Gyroid enantiomers, and structural disorder. Each of these factors weakens, but does not fully extinguish, the circular polarisation signal. We further find a substantial amount of blue-absorbing pigment in those wing scales of *C. rubi* that are structured according to the single Gyroid. Numerical simulations demonstrate that absorption, while evidently reducing overall reflectance, does generally not reduce the circular dichroism strength. The experimental findings of this paper, however, clearly demonstrate that circular dichroism is absent from the reflections of the butterfly wing scale. Henceforth, the chiro-optical response of the idealised structure does not fulfil a biological photonic function.

Selection and Peer-review under responsibility of Physics Department, University of Namur.

Keywords: circular polarisation, Gyroid, chitin, chirality, biophotonic crystals, optical activity, birefringence, butterfly wing scale, pigmentation, absorption, structural color

Phenomena related to circular polarisation (CP) have a history in biophotonic research going back to Michelson's observation ([1] , see also [2–4]) that the reflectance for left-circularly polarized light (LCP) from the cuticles of the scarab beetle *Chrysina resplendens* differs from that for right-circularly polarized light (RCP). Recent studies thereof have identified a cholesteric liquid crystalline structure as the origin [3,5–7]. Other examples for the relevance of CP for biophotonics include the bioluminescence of some firefly species [8], the CP sensitivity of the visual organs of the mantis shrimp [9–11] and the CP reflections of the *Pollia* fruit [12]. Experimental observations of CP effects in butterflies, both with respect to reflectance and to the sensitivity of the visual organs, have not been reported.

* M. Saba and B.D. Wilts contributed equally to this work.
** Corresponding author: Gerd Schröder-Turk (Email: gerd.schroeder-turk@fau.de)

Selection and Peer-review under responsibility of Physics Department, University of Namur.
doi:10.1016/j.matpr.2014.09.023

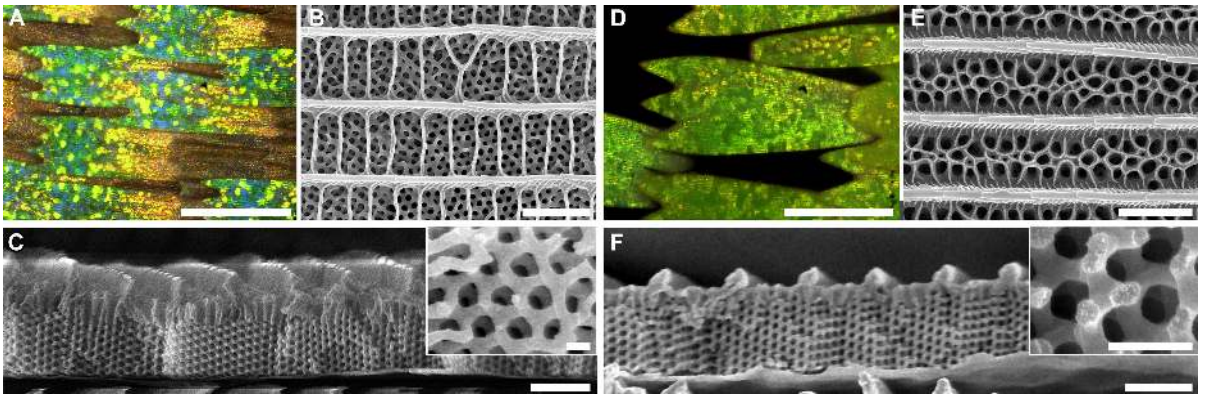

Fig. 1. **Optical microscopy and scanning electron microscopy of the wing scales of *Callophrys rubi* (A-C) and *Teinopalpus imperialis* (D-F):** Scale bars are 100 µm (A,D), 2 µm (B,C,E,F) and 200 nm (inserts of C,F). The light micrographs (A,D) reveal a tessellated appearance reflecting the poly-crystalline nature of the crystallites with different orientation of the Gyroid structure (B,C,E,F) within the wing scales.

However, the presence of the chiral ordered network-like nanostructure, known as the *single gyroid* [13] in the wing scales of several butterfly species including *Callophrys rubi* and *Teinopalpus imperialis* is well confirmed in the literature [14–20] [1] , with its contribution to structural color and iridescence widely recognised [20,24–26]. As an idealised dielectric material and in nanofabricated realisations thereof, this chiral single Gyroid structure shows a clear CP signal in transmission [27–29]. The presence of this chiral nanostructure naturally leads to the question if the wing scales of green butterflies structured according to the Gyroid exhibit macroscopic and biologically relevant CP reflections. We here set out to explore this question.

1. The single Gyroid geometry and its structural chirality

In the context of its realisation as a photonic material, the single Gyroid [13,30–32] is best described as a triply-periodic porous material with cubic symmetry, consisting of two components each of which is a single component with a network-like shape (here, one air-filled and the other one composed of solid chitin), see Fig. 2. Two commonly adopted perspectives describe the single Gyroid with reference to (a) the periodic net or graph, called **srs** [33], tracing the centerlines of the solid or void component [31], or (b) to the negatively curved interface, modelled as a minimal surface [32] or a constant mean curvature (CMC) surface [34], that separates the solid and the void component.

The single Gyroid is a chiral structure, manifest in its cubic symmetry group $I4_132$ with two-, three- and four-fold screw axes. Chirality – defined as the geometric property that an object's mirror image cannot be transformed by translation and rotation to coincide with the object itself – is evidently a property of the whole object, here of the triply-periodic net, which is infinitely large, in principle. However, it is instructive to identify different aspects of the chirality with local elements, in particular with subsets of the Gyroid net in the vicinity of the screw-axes that resemble discrete left- (LH) or right-handed (RH) helices. Fig. 2 (**C, D, F, G, I, J**) shows the helix-like arrangements of the **srs**-graph revolving around the screw axes in the [100], [111] and [110] lattice directions. It turns out that, for the situation where the solid phase is given by a CMC representation of the Gyroid surface with approximately 20% chitin volume fraction, the screw axes are either fully in the void phase of the Gyroid porous material or go through the solid phase. We hence classify these screw axes, and their corresponding helical elements, as either *centered in the solid phase*, or *solid* for short, (Fig. 2 **C, F, I**) or *centered in the void phase* (Fig. 2 **D, G, J**). We reiterate that this

[1] The presence of the chiral Gyroid nanostructure in the wing scales of *Callophrys rubi* [14,16–18] and *Teinopalpus imperialis* [14,15] (see Fig. 1, and also earlier work in [21]) and, albeit not the subject of this study, *Callophrys gryneus* [15], *Callophrys dumetorum* [15], *Cyanophrys heredotus* [15], *Parides childreanae* [19] and *Parides sesostris* [14,15,20,22], suggests the possibility of circularly polarized reflections of the Gyroid-structured wing scales of these species. Note also that the structure in *Cyanophrys remus* (a butterfly which has by now been reclassified as part of the *Callophrys* family) identified as an inverse opal [23] may also be a single Gyroid structure.

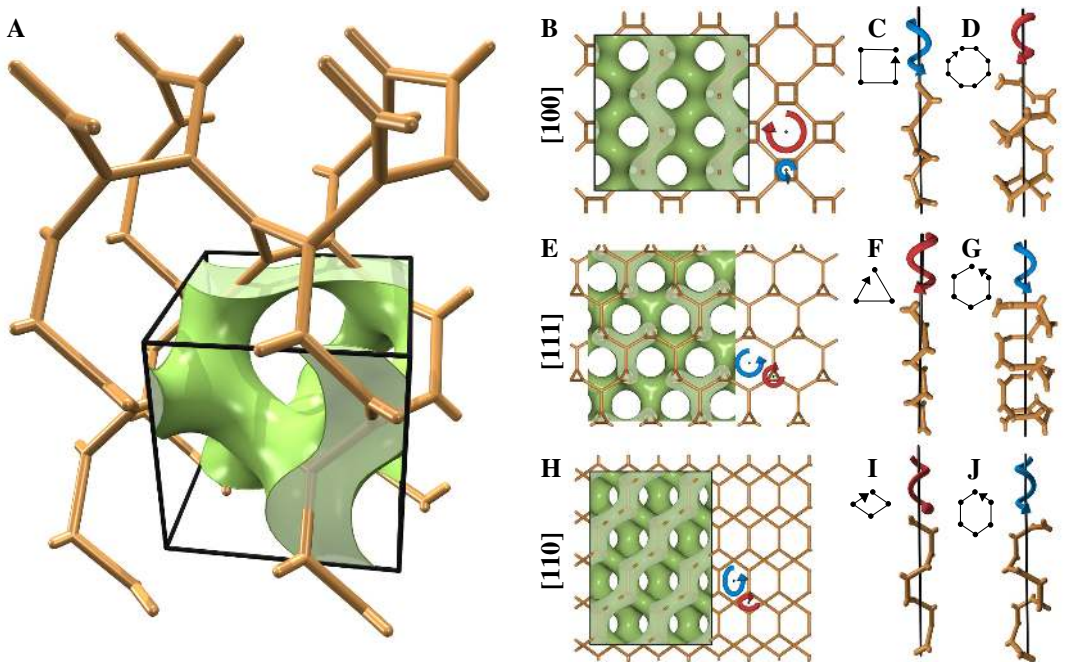

Fig. 2. **Subtleties of the structural chirality of the single Gyroid morphology: A** Perspective view of the **srs** net (orange) and of a CMC single Gyroid structure with volume fraction $\phi \approx 20\%$ (green). **B-D** projection along the crystallographic [100] direction and perspective views of the helical elements along this direction, i.e. of subsets of the **srs** net contained in cylinders around the screw axes. The RH helix (**D**) with an octagonal cross-section, with the screw axis centered in the void space, is composed of 8 edges (per cubic unit cell), with alternating horizontal ('h') and inclined, or skew ('i') edges ('h' denotes an edge that is horizontal (i.e. perpendicular to the axis), 'v' an edge that is parallel to the axis and 'i' an inclined edge that is neither 'v' nor 'h'). The LH helix (**C**) with square cross-section, whose screw axis is centered in the solid domain, is composed of four edges, all of type 'i'. **E-G** [111] direction, 3_1 screw axes: The RH screw axis (**F**) is centered in the solid and has triangular cross-section; all 3 edges are type 'i'. The LH element (**G**) corresponds to the screw axis centered in the void, has hexagonal cross-section and is composed of 9 edges, following a sequence h-h-i. **H-J** [110] direction, 2_1 screw axes: The RH element (**I**), corresponding to a screw axis that is centered in the solid, is a helical element with rhombic cross-section composed of 6 edges, with a sequence i-i-v. The LH element (**J**), corresponding to a screw axis centered in the void, has a six-sided cross-section (an distorted hexagon) and is composed of 8 edges with sequence h-i-v-i.

is merely a geometric classification, as the chirality is evidently a property of the overall geometric structure, rather than of its local elements.

While the single Gyroid geometry is clearly chiral, its chirality is subtle and confounded by two issues:

Presence of LH and RH 'solid' chiral elements in different lattice directions The handedness of the screw axes that are centered in the solid is different for the different lattice directions. For the enantiomer where the solid screw axis along the [100] direction is left-handed (as in Fig. 2 **C**), the helical elements along the [111] direction and along the [110] direction are RH (Fig. 2 **F, I**).

Presence of 'solid' and 'void' helical elements of opposite handedness in each lattice direction In each of the three lattice directions [100], [111] and [110], screw axis (and their corresponding helical elements) of different handedness exist. In each direction, solid elements with a smaller average radius of the helical element (Fig. 2 **C,F,I**) compete with screw axes centered in the void (Fig. 2 **D,G,J**) that correspond to helical elements with larger radius and of the opposite handedness.[2]

[2] In a related context, note the even more subtle chirality of the synthetic **4-srs** photonic crystal, composed of four equal-handed Gyroid nets. In the space group of the **4-srs** $P4_232$, a single 4_2 screw axis along the [100] direction is at the same time RH and LH. The only difference between the two rotation senses is the topological continuity of the effect of the screw motion on the **4-srs** geometry (cf. [35]).

For the photonic computations presented below we define the Gyroid as the volume enclosed by its nodal surface approximation that is given by (cf. [36], with $G = 2\pi/a$ denoting the reciprocal lattice parameter and a the lattice parameter of the single Gyroid in its space group $I4_132$)

$$t > \sin Gx' \cdot \cos Gy' + \sin Gy' \cdot \cos Gz' + \sin Gz' \cdot \cos Gx' \tag{1}$$

with the position vector $\vec{r}$ rotated to $\vec{r}' = (x', y', z')$ such that the respective inclination normal (either [100], [110] or [111]) is parallel to $\vec{e}_z$. The separation threshold t determines the volume fraction ϕ of the channel. In the following we set the volume fraction to $\phi \approx 20\%$ (which is at the lower end of estimated volume fractions for the Gyroid phase within *C. rubi*'s wing scales, see [16]) corresponding to a separation threshold $t \approx -0.9$ [36].

The frequency dependence of the photonic properties analysed below (Figs. 5 to 7) is given both as a function of the (vacuum) wave length λ_0 of the incoming light as well as the reduced frequency $\Omega = \frac{a}{\lambda_0}$. The use of Ω is motivated by the scaling properties of the Maxwell equations[3] stating that the photonic response of a frequency independent material as a function of Ω is conserved under a change of the lattice parameter $a \to r \times a$ (i.e. an affine rescaling of the structure size with a real number r): A nano-structure with lattice parameter $r \times a$ has the same response for incoming light of wavelength $r \times \lambda$ as a similar structure with lattice parameter a has to incoming light with wavelength λ. In Figs. 5 to 7, we have set to $a = 311$ nm in line with experimental data from [16].

2. Chiral-optical properties and circular polarisation

The chiral-optical properties of the single Gyroid have been the subject of recent studies: band structure analysis and simulation have demonstrated that, as a dielectric lossless material, the single Gyroid exhibits a 'circular polarisation stop band' along the [100] direction [35], see also Fig. 5(left); this finding has been largely corroborated by optical measurements on nanofabricated specimens, both with dielectric material constants $\varepsilon = 1.58$ similar to the butterflies chitin material [27,28] and with higher refractive index Chalcogenide glasses ($\varepsilon = 5.7$, [29]). (The fact that a CP band gap, if existent, would likely occur in a higher frequency range above the visible was predicted [25], however without corroborating evidence or citation). When realised as a gold meta-material (possible by duplicating from the alternating Gyroid phase in triblock copolymeric self-assembly [37]), it shows optical chirality and circular polarisation effects [37,38], albeit of a smaller magnitude than its chiral structure may have suggested [39]. The optical properties of the achiral *double Gyroid*, composed of two intergrown network domains separated by a void matrix, has been studied widely, as a UV protection mechanism in retinal microlenses in tree shrews [40], as dielectric materials [36,41] and plasmonic materials [38], and as a possible realisation of Weyl points [42]. Various optical properties of the single Gyroid that are not related to circular polarisation have been addressed, in centimeter scale specimens in the microwave regime [43] and by simulation [36,41].

Circular birefringence or optical activity (OA) and circular dichroism (CD) are polarisation effects related to the chiral properties of a light-transmitting medium. In the literature, OA is the ability to rotate the semi-major axis of elliptically polarized light, and CD corresponds to the difference in the absorption coefficients between LCP and RCP light for a homogeneous or homogenized medium [44]. Thus, while OA describes a scattering phenomenon, CD is traditionally connected to a material constant. However, OA can also be directly correlated to a difference in refractive index for RCP and LCP modes[4] in a homogeneous medium. On the other hand, scattering at a structure with finite CD causes a change of the eccentricity of the polarization ellipse. Here, we therefore quantify CD by its impact on the scattering parameters as the relative difference between the absolute values of the complex reflection amplitudes $r_\pm$ for a respective incoming LCP (+) or RCP (−) plane wave (as in [47]):

$$\mathrm{CD} = \frac{|r_+| - |r_-|}{|r_+| + |r_-|} \tag{2}$$

[3] This is a result of all four equations being first order differential equations in time and space and true as long as the material properties encoded in the constitutive equations are frequency independent (e.g. $\varepsilon(\Omega) = \text{const.}$).

[4] Those are eigenstates of a chiral medium modeled by a set of bi-isotropic constitutive relations with vanishing reciprocity [45,46].

In this paper we present experimental data demonstrating that there is no discernible CD signal in the reflections of macroscopic portions of the wing scales of the green-colored scales of *Callophrys rubi* and *Teinopalpus imperialis*, both having a single Gyroid photonic crystal (see section 3). This absence of a CD signal is somewhat at odds with the evidence that, as a material, the single Gyroid structure produces this signal. We have been unable to find a single reason that annihilates the CD signal, but will discuss the following factors, all of which might contribute to a reduction of CD strength:

Orientation effects (section 4) The structure in the wing scale is a poly-crystalline assembly, with individual grains adopting different orientations. The CP effect, which is only of substantial strength along the [100] direction, is weakened by the contribution of the unpolarized reflections of the other orientations.

Presence of an absorbing pigment (section 5) The presence of substantial quantities of an absorbing pigment reduces the overall strength of reflections. Numerically, However, we find no substantial reduction in the circular dichroism strength.

Lack of enantiopurity The single Gyroid can be realised in two enantiomeric forms (one called LH, the other called RH), being mirror images of each other. While preliminary studies suggest a 1:7 prevalence of one of the two enantiomeric forms [18], the presence of both enantiomers weakens the CP signal.

Structural disorder The single Gyroid provides a close approximation of the porous structure of chitin in the butterfly wing scales, yet structural disorder (both high- and low-frequency modulations) or defects are present.

Sensitivity to incident angle variations and breakdown of the plane wave approximation As a body-centered crystalline structure, the photonic properties along the CP-sensitive [100] direction are sensitive to small variations of the incident angle. Similarly, the CP signal may be weakened when the incident light is not well approximated by a plane wave.

Effect of the rib-structure (*C. rubi*) or honeycomb structure (*T. imperialis*) above the single Gyroid The distance between the thinner ribs is $\approx 600\,\mathrm{nm}$ in *C. rubi*, see Fig. 1B. This structure could provide a photonic effect that suppresses the circular-polarisation signal of the underlying Gyroid photonic crystal.

The absence of the overall CP signal is likely to be a compound effect of these factors, reducing the signal strength below the experimentally observable strength, and making it highly unlikely that it fulfils a biological purpose.

3. Measurement of circular-polarisation of reflectance of butterfly wing scales and beetle exoskeletons

We have performed spectrally resolved measurements of the reflectance for circularly polarized light for the wing scales of *C. rubi* and *T. imperialis*, at normal incidence, separately for RCP and LCP light. Only cover wing scales with green appearance (that, in contrast to the melanin-containing black-colored ground scales), contain the single Gyroid nanostructure) were considered.

Two beetles with known circularly polarized reflectance [2,48,49] were used to test the measurement system: first, a broad-band reflecting, silver-colored *Plusiotis optima* (Rutelinae) and the narrow-band, green colored *Canthon fulgidus* (Scarabaeinae). Whereas the colour of both beetles is largely different, both exocuticles of these beetles strongly preferentially reflect LCP light in a mirror-like fashion (see Fig. 3**A**). The reflection of RCP light is minor, and no sign of constructive interference can be observed in this channel. The differential response to LCP and RCP light is due to a chiral, left-handed assembly of chitin layers in the exocuticle, which is either well-ordered and acts as a narrow-band interference reflector (*Canthon fulgidus*) or chirped and acts as a broad-band interference reflector (*Plusiotis optima*) [5,50,51]).

Figure 4 demonstrates that, in contrast to the reflections of the beetle exoskeletons, no significant difference between the LCP and RCP reflectance can be observed for green-colored wing scales of *C. rubi* and *T. imperialis*, despite the presence of the chiral Gyroid structure in their wing scales (cf. Fig. 1). The illuminated measurement area was approximately $6\,\mu\mathrm{m} \times 6\,\mu\mathrm{m}$. Given that the typical linear extent of a single crystallite is typically around $3\,\mu\mathrm{m}$, the measurements integrate the reflection of only a few crystallite domains.

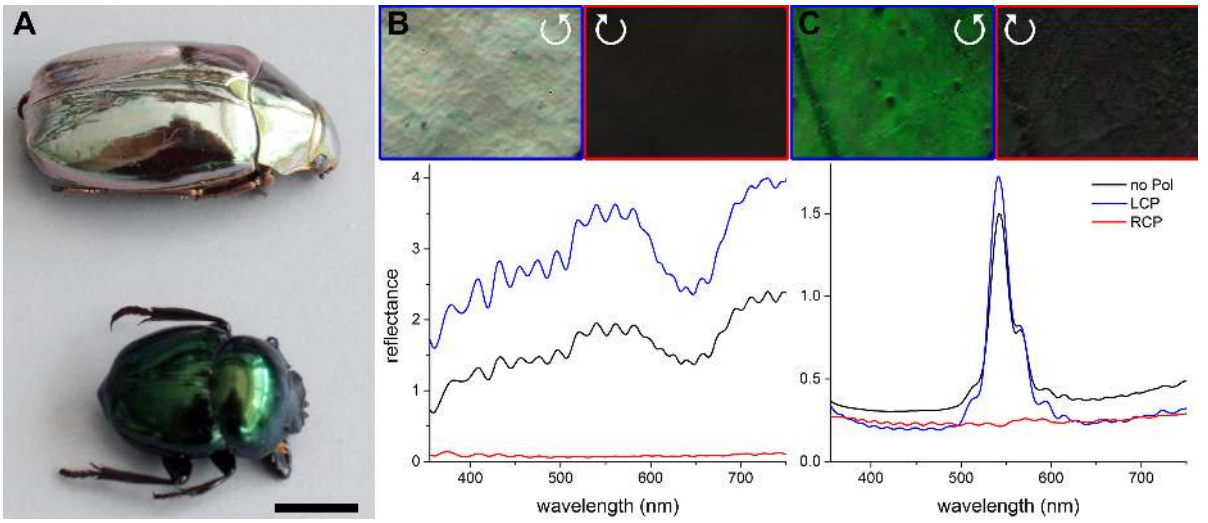

Fig. 3. **Circular-polarisation resolved reflectance measurements for the beetles *Plusiotis optima* and *Canthon fulgidus*:** (A) Photographs of the silver-colored *Plusiotis optima* (top) and the green-colored *Canthon fulgidus* with unpolarized light. Note the mirror reflection of the photographer visible on the cuticle of the *P. optima* specimen. (B,C) Circular-polarisation dependent reflectance measurements for *P. optima* (B) and *C. fulgidus* (C) confirm the chiral, left-handed nature of the photonic structure inside the beetle exoskeleton (see sect. 7.3 for experimental details). The measurement area for the reflectance spectra was 6 µm × 6 µm. The light photographs above the spectra are light-microscopy reflectance images for LCP and RCP incident white light.

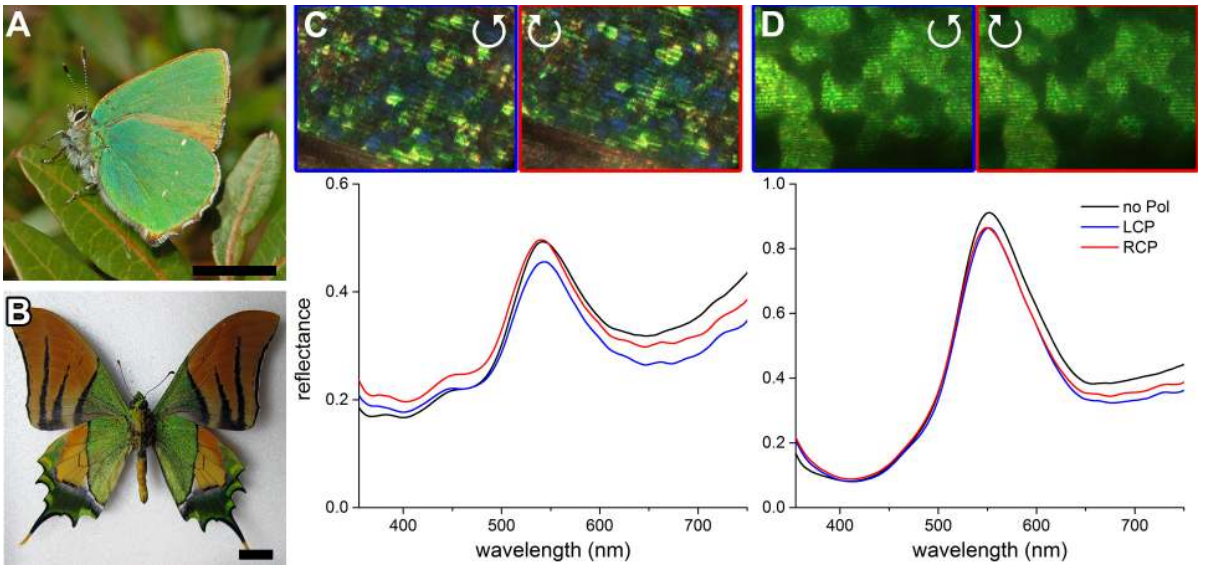

Fig. 4. **Circular-polarisation resolved reflectance measurements for the butterflies *C. rubi* and *T. imperialis*:** (A) Habitat photographs of *Callophrys rubi* (scale bar: 1 cm, photograph in the public domain). (B) Photograph of the ventral side of Teinopalpus imperialis (scale bar: 1 cm, photograph in the public domain). (C,D) Circular-polarisation dependent reflectance measurements for *C. rubi* (C) and *T. imperialis* (D) show no CD. The measurement area for the reflectance spectra was 6 µm × 6 µm. The light photographs above the spectra are light-microscopy reflectance images for LCP and RCP incident white light.

4. Orientation effects and polycrystallinity: Circular polarisation in single Gyroid along different crystallographic axes

It is well known that the Gyroid structure in the wing scales of *C. rubi* is polycrystalline with relatively small crystal domains (≈10 unit cells laterally) with different inclinations (i.e. crystal orientation with respect to the structure

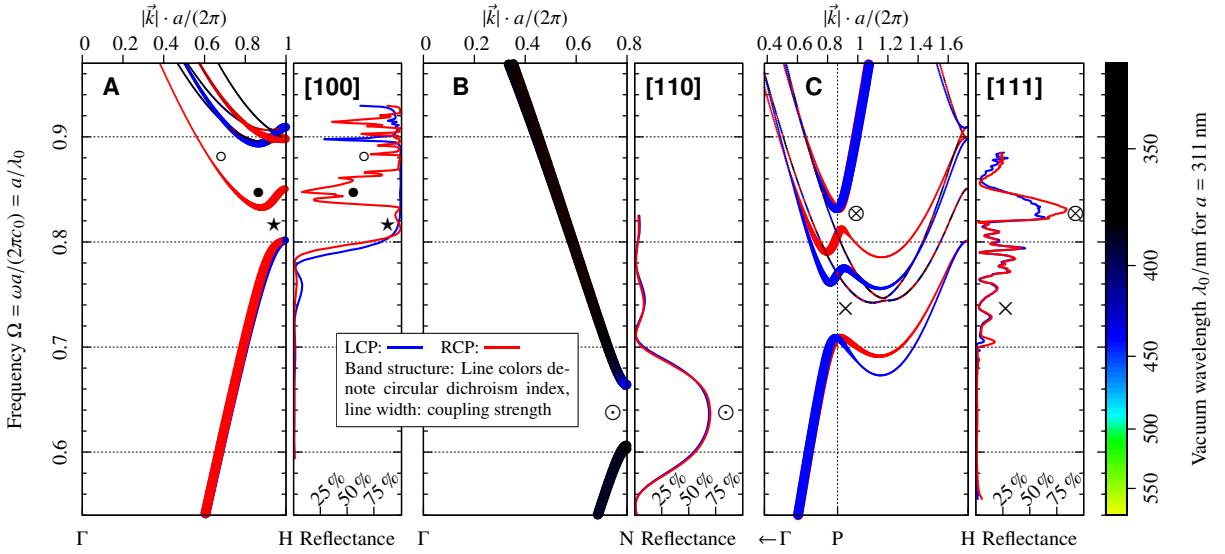

Fig. 5. **Direction dependence of the circular dichroism of the single Gyroid structure:** Circular dichroism along different crystallographic directions is quantified by the bulk band structure (left parts, colouring encodes dichroism index and line width coupling strength as defined in [35]; Capital letters at the bottom denote boundaries of the Brillouin zone at high-symmetry points [52]), and by FDTD simulations of the reflectance (right parts, averaged over finite sheets of Gyroid material of thickness $5.5 \cdots 6.1 \times a$, and terminations $z_T = 1/30, 4/30$, cf. sec. 7.5). The single Gyroid is modelled by the nodal approximation (eq. (1)) with $t = -0.90$, corresponding to a volume fraction of solid chitin of $\phi \approx 20\,\%$; the dielectric constant is $\varepsilon = 2.4$. Frequency regions that are labelled with symbols are discussed and referenced in the main text.

surface on top of the wing scale) [14,18]. Statistics on the probability of different inclination planes has not been published in the case of *C. rubi*. A similar study, however, has revealed that the [110] inclination is predominant in the case of *P. sesostris* [20].

The open question of crystal orientation is of great importance for this work as the structural color signal and also the circular dichroism of the Gyroid photonic crystal is highly anisotropic. We do not provide the missing statistics for *C. rubi* here; however, TEM micrographs from previous works (e.g. [16,18]) indicate that inclinations at distinct high symmetry directions are present.[5] Furthermore, we assume that the crystal domains are still large enough so that the reflectance can be modelled by the weighted sum over the reflections that the different domains produce. In Fig. 5 we therefore show the band structure and the circular dichroism and coupling index [35] along the [100], [110] and [111] directions and the reflection spectra for left and right circular polarized plane waves at normal incidence from a finite Gyroid slab of corresponding inclination. We find the following main features for the three crystal directions:

[100] direction – Band gap and circular dichroism stop band A similar plot to Fig. 5**A** for different volume fraction and dielectric contrast has been previously published in [35]; for all three directions we have used the same coloring for the circular dichroism index and the same point size for the coupling index as in [35]. A band gap where both polarizations are reflected is present at $0.8 < \Omega < 0.83$ (marked by symbol ⋆in Fig. 5**A**) in the near UV. Significant CD is found directly above that band gap around $\Omega = 0.85$ (•), i.e. at wavelengths below 380 nm.[6]

[110] direction – primitive direction with no circular dichroism Fig. 5**B** corresponds to the direction of a primitive reciprocal lattice vector of the body-centered cubic Gyroid. Therefore, the behaviour resembles a simple

[5] This is also evident from the different colors of the domains in Fig. 1**A** and 4**C**.

[6] Note that there is a sign error in our previous analysis [35], related to the group velocity, that is corrected here (and also in [28]): For example, there is no color switch from red to blue for the band that causes the CD in contrast to the previous findings in [35]. The corrected dichroism index explains the transmission spectrum above $\Omega = 0.85$ (○) better, where the RCP coupling band coincides with the reflection for RCP light being still clearly below one.

multilayer structure, and exhibits a band-gap around $\Omega \approx 0.65$ ($\odot$, ≈ 490 nm, green-blue), similar to fig. 4a in ref. [53] of the same structure and inclination, but with different parameters. The circular dichroism is negligible which is demonstrated by the band structure as well as the reflectance spectrum. This is the predominant orientation found in the wing scales of *P. sesostris* in [20] and henceforth no circular polarization effect is expected for this specific butterfly. A similar study for *T. imperialis* would provide further clues for the absence of CD in this species (cf. Fig. 4).

The reflection caused by this band gap is likely to be the major contributor to the green-blueish coloration of the butterfly. The slight shift in the position of the reflectance maximum between experimental data in fig. 4 (540nm) and this theoretical modeling (490nm) may be a consequence of the use of a lower estimate for the lattice constant a and the volume fraction ϕ, as noted above. Variations of these parameters would likely cause a red-shift towards the green wavelengths (note also the data in Fig. 4a of ref. [53]).

[111] direction – no band gap, but stop band with minor circular dichroism It is not sufficient to consider the band structure within the first Brillouin zone from Γ to P ($\vec{K} := \vec{k}a/(2\pi c) = (1/2, 1/2, 1/2)^T$) to identify partial band gaps for the [111] direction (Fig. 5**C**). It turns out that we need to follow the [111] direction until the H point (cf. [100] direction, Fig. 5**A**) is reached at $\vec{K} = (111)^T$.[7] This complication has not always been taken account for in previous works, see for example Fig. 6 of [25] where partial band gaps that do not exist in most of the directions are shown for a nodal surface Gyroid with $t = 0$ and a refractive index of $n = 1.5$. Note, that their band gap in [111] direction corresponds to the region $0.71 < \Omega < 0.76$ ($\times$, ≈ 430 nm, blue) in Fig. 5**C** where no band gap is visible in the extended zone scheme. We find relatively small CD compared to the one that seen in Fig. 5**A** at roughly the same frequency around $\Omega = 0.825$ ($\otimes$, ≈ 380 nm, near UV) where the reflection is largest for both polarizations. However, no photonic band gap is present in the frequency range of interest and henceforth no coloring (except for a small amount of light reflected in the UV) is caused by the [111] inclined crystal.

Many of the effects, especially in the [111] direction, are too complicated to be understood by a single mode coupling index and require a full scattering analysis involving multiple modes, including those which are evanescent (and hence not seen in the ordinary band structure). For example, the reflectance is relatively small even though no strong coupling bands are exist in the frequency region $0.71 < \Omega < 0.76$ and [111] direction ($\times$). A currently unpublished new method to calculate the band structure, including evanescent modes with complex wave vector, of arbitrary triangulated geometries [54] reveals evanescent modes with a small imaginary part of the wave vector that are strongly coupling and can hence work as a transmission channel or as a communication channel between an incident plane wave and the non-evanescent Bloch modes. These modes are also present in the [110] direction in the band gap ($\odot$) where the reflection is therefore less then 70% but not in the [100] direction at $0.8 < \Omega < 0.825$ ($\star$) where the reflectance as a result reaches almost 100% despite the small width of the band gap here.

5. Presence of absorbing pigment in green wing scales with Gyroid nanostructure

Previous measurements on butterfly wing scales structured according to the single Gyroid geometry [26] have shown that pigments may be present.

To measure whether this is also the case for the wing scales of the Green Hairstreak we measure the transmittance of single wing scales in air and in refractive index-matching oil, with refractive index $n = 1.6$ (Fig. 6) with a microspectrophotometer. When no immersion fluid is applied, individual domains of Gyroids crystals can be identified (Fig. 6**A**). After immersion in refractive index-matching fluid (Fig. 6**B**), light scattering is suppressed. If no pigment is present in the solid nano-structure of the scale, the scale appears transparent in index-matching fluid, leading to no

[7] Generally, for a direction with Miller indices [hkl] we need to follow the straight path until another Gamma point is reached to cover all modes that potentially couple to an incident plane wave propagating in [hkl] direction. In practice, half of this way is enough because of time-reversal symmetry for lossless structures so that the end point is at $\lambda/2 \times (hkl)^T$ that is determined by the equation $\lambda \times (hkl)^T = \vec{G}$ for an unknown λ and the smallest possible reciprocal lattice vector $\vec{G}$. For [hkl] = [111] in the body centered cubic case that yields $\lambda = 2$ so that the end point is $\vec{K} = (111)^T$ which is equivalent to the H point at $\vec{K} = (100)^T$ in the first Brillouin zone.

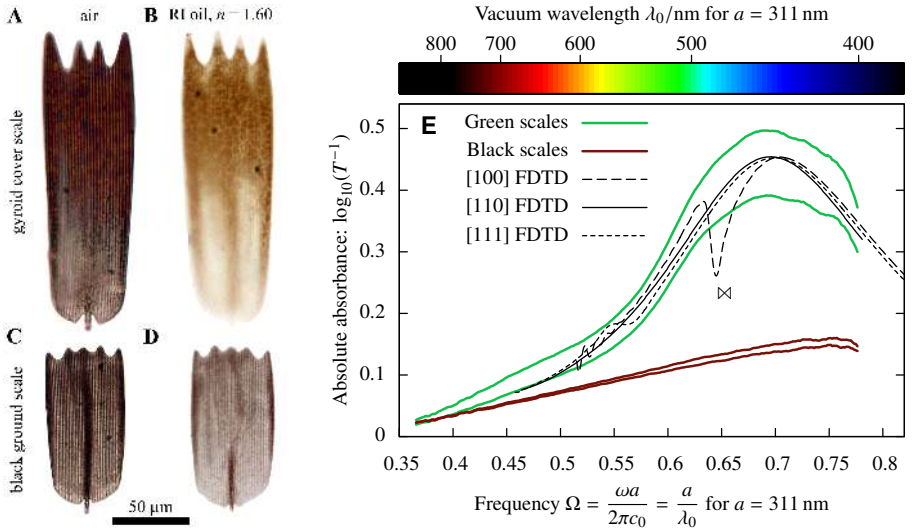

Fig. 6. (Color Online) **Absorbance of *Callophrys rubi's* wing scales and corresponding complex dielectric contrast**: (**A**,**B**) Transmission photographs of Gyroid cover scales in air (**A**) and an refractive index (RI) matching fluid with $n = 1.6$ (**B**). Single domains are clearly visible at the tip of the wing scales. Immersion of the wing scales in refractive index fluid diminishes light scattering and allows a quantitative measurement of the absorbance of pigments immersed in the wing scale. (**C**,**D**) Transmission photograph of black ground scale in air (**C**) and in RI oil (**D**). (**E**) Absorbance spectra of green and black wing scales show the presence of melanin in the black scales (brown lines) and the presence of an unknown blue-absorbing pigment in the Gyroid photonic crystal domains (green lines). The Gyroid scale curves are matched by numerical FDTD experiments of a Gyroid material of layer thickness $6a \approx 1.9\,\mu$m, with constant refractive index n and a Lorentz absorber in the Gyroid domain, and lossless dielectric of same refractive index filling the hollow channel, differently inclined (black lines). If the structure is aligned in [100] direction, a resonance in the absorbance ($\bowtie$) is observed at $\Omega = 1/n$ where the medium wavelength matches the lattice constant of the Gyroid. The physical origin of this resonance remains unclear.

colored reflections from the individual domains. In the case of Gyroid-containing *C. rubi* scales, however, a mosaic of brown-yellow colour remains co-localised with the Gyroid domains, strongly hinting at the presence of a blue-absorbing pigment in these domains. By contrast, for the black ground scales (shown in Fig. 6**C,D**) the immersion in index-matching fluid leads to a much weaker spectral effect, reminiscent of melanin (see below), showing no sign of the presence of a blue-absorbing pigment.

Pigments are often found in butterflies and are the source for most patterns in nature [55–59]. Most commonly, pigments are found in unstructured scales and are not co-localised with photonic structures. Pigments typically only act as contrast enhancers (by absorbing light, [12,15,26]) or as an additional color signal for chromatic contrast [58,60]. A combination of photonic structures and pigments within the same scales appears to be rare and has so far only been identified in the wing scales of *P. sesostris* [26] and butterflies of the *nireus* group [61], as well as in bird feathers [62,63].

Further support for the presence of an absorbing pigment is provided by the measurement of transmittance spectra $T(\omega)$ of isolated scales that yield the absorbance spectra $A(\omega) = -\log_{10}(T(\omega))$,[8] see Fig. 6**C**. The spectra reveal a distinct short-wavelength-absorbing pigment with a peak absorbance of $A \approx 0.5$ at 450 nm. The transmittance spectra of the black ground scales (situated below the Gyroid cover scales) is flat and monotonously increasing for longer wavelengths, very reminiscent of melanin (brown lines in Fig. 7**C**, cf. [64]). The presence of an absorbing pigment in the green wing scales of *C. rubi* has so far not been noted in the literature. (These findings suggest to study the effect of finite absorption within the Gyroid domain on the strong circular dichroism that is found around $\Omega = 0.85$ for the [100] inclination (Fig. 5). The dispersion of chitin and the absorption of the blue-absorbing pigment is modeled by a

[8] With the reasonable assumption that no significant fraction of the light is reflected by the immersed structure. While there is no theoretical evidence that reflection is strictly zero it is below 2% for all frequencies in the numerical experiment.

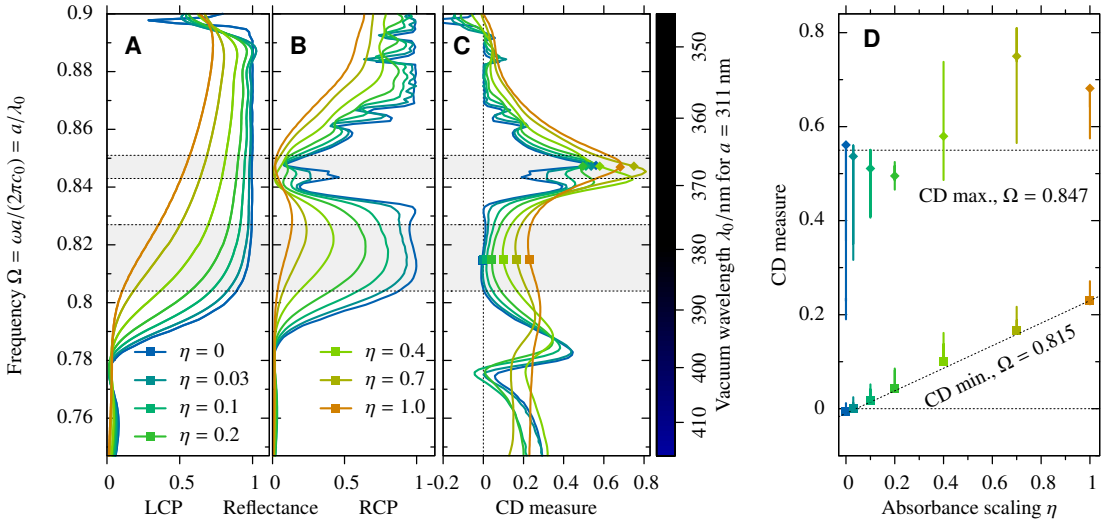

Fig. 7. Reflectance spectra (**A, B**) of [100]-inclined FDTD simulations of a Gyroid structure with $\varepsilon = 2.4$, $\phi = 0.21$, and Lorentzian absorbance scaled by $\eta \in [0; 1]$, as of eq. (3). Subfigure **C** presents the value of the Circular dichroism measure introduced by eq. (2) in section 2; positive CD is synonymous with excess LCP reflectance. At the fixed frequencies $\Omega = 0.815$ (CD minimal, squares) and $\Omega = 0.847$ (CD maximal, diamonds), respective symbols are drawn onto the CD measure curve **C** as well as to the CD-vs.-absorbance summary graph **D**. The CD of the frequency intervals around the extrema (shaded within **A..C**) is depicted in **D** collapsed into colored lines at the appropriate absorbance η. There, the symbols depict the CD at the chosen frequency, whereas the lines visualise the CD within the narrow frequency range where no qualitative change in behaviour of CD index occurs, and are therefore more robust against small frequency shifts and line shape changes. Dashed lines are guides to the eye.

material made of Lorentz oscillators for which the permittivity is given by

$$\varepsilon(\eta, \Omega) = \varepsilon_\infty + \eta\,\sigma_\mathrm{L} \frac{\Omega_\mathrm{L}^2}{\Omega_\mathrm{L}^2 - \Omega^2 - \imath\,\Omega\,\gamma_\mathrm{L}} \tag{3}$$

with the limit refractive index $n_\infty = \sqrt{\varepsilon_\infty} = \sqrt{2.4}$, the resonance frequency $\Omega_\mathrm{L} = 0.695$, the damping constant $\gamma_\mathrm{L} = 0.26$ and the resonance strength $\sigma_\mathrm{L} = 0.1117$ (with an absorption modifier η).[9] A numerical experiment with $\eta = 1$ where the Gyroid made of this artificial material is *immersed* in a dielectric with ε_∞ yields the absorbance curves shown in red in Fig. 6**C** for the different inclinations. Except for a resonance phenomenon (marked by ⋈in Fig. 6**C**) in the [100] direction, they match the measured data well.) The reflectance spectra of the Gyroid in air with different absorption modifiers η (ranging from vanishing absorption $\eta = 0$, cf. Fig. 5**A** to full absorption $\eta = 1$ corresponding to the experimental data fit in Fig. 6) is shown in Fig. 7**A** (LCP) and **B** (RCP). For most frequencies, the reflectance decreases with increasing η. Finite absorption also removes resonance effects (Fano and Fabry-Pérot) that are due to the finite size of the Gyroid slab even for relatively small η. Both phenomena are expected by theory. The different magnitude of the decrease of reflectivity for the two polarizations yields a change in circular dichroism strength $\mathrm{CD} = (\sqrt{R_\mathrm{LCP}} - \sqrt{R_\mathrm{RCP}})/(\sqrt{R_\mathrm{LCP}} + \sqrt{R_\mathrm{RCP}})$ (see eq. (2)) and is illustrated in Fig. 7**C**. We illustrate the CD as a function of η for the interesting CD maximum in the vicinity of $\Omega = 0.847$ and a local CD minimum at $\Omega = 0.815$ in Fig. 7**D**. As the absorption strength also induces frequency blue (or red) shifts in the CD spectrum, we depict the adjacent frequency range (shaded within subfig. **C**, as lines) alongside the values at the fixed frequencies (symbols). That way the shift of local extrema with varying η becomes visible, rather than relying on less robust extremum-search methods.

[9] A more realistic model would include at least one additional term for a frequency dependent real part [65] of ε (connected to high frequency absorption beyond the near UV of the chitin itself). However, this is a detail that does not amend the general conclusions and is likely to be outbalanced by other uncertainties such as the material volume fraction and structural disorder.

Importantly, the key result of Fig. 7 is that the presence of an absorbing pigment does not lead to a significant reduction of the CD strength near $\Omega = 0.847$ in the CD band gap. It is indeed noteworthy that at lower frequencies around $\Omega = 0.815$, the system exhibits a finite CD signal proportional to the absorbance.

6. Conclusion and Discussion

We have demonstrated, by reflectometry measurements on the Gyroid nanostructured wing scales of *C. rubi* and *T. imperialis*, that macroscopic reflectance of the wings of these butterflies is equal for both LCP and RCP light, despite the presence of the chiral Gyroid nanostructure in the wing scales.

Noteworthy, our reflectometry measurements are circular-polarisation sensitive within range that extends to wavelengths well below 400 nm, outside of the visible spectrum for human vision, where the circular-polarisation signal for the single Gyroid photonic crystal is expected [35]. In this context, note the previous analysis by Mille *et al.* [18] that analysed reflectance data for wavelengths above ≈ 420 nm and observed no CP effects; however, that study identifies individual crystallites in wing scales of *C. rubi* that appear to show CP effects in the green (see Fig. 10 in ref. [18]).[10]

The absence of a CP signal in the reflectance measurements appears to be paradox because the circular-polarisation effects of the single Gyroid structure are well documented, both by theory [35] and by experiments [27–29]. To resolve this paradox, we have considered several factors that may cause the CP signal to disappear or fade below the accuracy of our measurements. The likely most important effect relates to the poly-crystallinity of the wing scale structure, with crystallites having different orientations; only the crystallites with inclination corresponding to the crystallographic [100] direction perpendicular to the wing surface shows a significant CP signal. Because of the size of the crystallites, which is around 3 μm in diameter, i.e. large compared to the wavelength of light, we consider the macroscopic response well approximated by the weighted arithmetic average of the contributions of the individual crystallites. The contributions from the [110] direction (and possibly other less symmetric inclinations) that are not circularly-polarized hence statistically weaken, but not extinguish, the CP signal from the crystallites with [100] and [111] inclination. If the prevalence of Gyroid crystallites with [110] inclination reported by Yoshioka *et al.* [20] for the butterfly *P. sesostris* (and also observed in epitaxial growth of copolymer Gyroid phases [66]) applies also to the species studied here, the contributions from the non-circular-polarising axes would be dominant compared to the contribution from the circularly-polarising [100] direction. An interesting experiment to further address this question of poly-crystallinity would be the analysis of microscopy images (such as those shown in Fig. 4) for monochromatic incident light with the frequency of the circular-polarisation response of the [100] direction.

The presence of absorbing pigments reduces the overall reflectance. However, this overall decrease in reflectance does not reduce the circular dichroism strength. Interestingly, measurements on *C. rubi* scales immersed in index-matched fluid show that a greater amount of absorbing pigment is present in the green scales (that are structured according to the single Gyroid) than in the black scales (which do not have a Gyroid structure).

Another factor that might also play a role is due to the experimental setup itself. While we idealise the source to be a plane wave at normal incidence in the simulations, the sample is rather illuminated by a light cone with an opening angle of $\approx 15°$ in the experiment. The angle of incidence is eminently of great importance as the CD is largest for the [100] direction which is particularly sensitive for small variations in the direction of the wave vector (cf. [47] page 14 and Fig. 7).

Our principal conclusion is the realisation that the Gyroid structure in green butterflies does not lead to macroscopic biologically-relevant circularly-polarised reflections, despite its structural chirality. This result falsifies the tempting hypothesis that the chiral single Gyroid structure is the result of the evolutionary development of a circularly-polarising communication channel, facilitated by circularly-polarising reflections of the wing scales. This leaves us to address the broader questions: Why does the single Gyroid structure form in butterfly wing scales in the first place? Does its chirality have a biological purpose at all?

[10] The experiment is however neither directly related to CD or OA: The authors show an optical micrograph of a sample illuminated under linear polarized light of unspecified azimuthal angle and use CP analyzer. The linear polarized incident beam prohibits a comparison with our CD simulations even if time reversal symmetry is applied.

In this context, it is important to realise that closely related achiral structures, comprised also of a single triply-periodic solid domain with a network-like topology, are also observed in the animal kingdom, in particular the achiral single Diamond structure in the exoskeletons of various beetles and weevils [22,67,68].

Several aspects of both the single Gyroid and single Diamond chitin structures indeed hint at the hypothesis that they result from evolutionary development towards efficient photonic biomaterials: The chitin volume fraction of single Gyroids in butterflies is close to the value giving the widest band gap [43], the layer thickness within the wing scale is parsimonious in the sense that thicker layers would not lead to a stronger signal [69] and the reflectance spectra appear to match those of the natural habitat (cf. Fig. 5 in ref. [22]).

However, another important consideration apart from photonic properties is the formation mechanisms of the single Gyroid and the single Diamond structures. The formation of these solid chitin structures is likely to be a two-stage process where intracellular cubic membranes structured according to the double Gyroid or the double Diamond form in the developing scales of the pupae and then solidify by selective deposition of chitin into a single network structure ([15,70], see also [16,71]). In such intracellular membranes, both the Gyroid and the Diamond geometry occur frequently in various kingdoms of life [72,73], likely for reasons of structural homogeneity [74,75] and spatial connectivity that are well understood within the corresponding physical chemistry self-assembly process of synthetic lipids [75]. This formation process emphasises the possibility that factors other than photonic effects may play an important role in the selection (by evolution or physical chemistry) of the resulting structure.

The formation process by cubic membranes certainly hints at the close similarity of the achiral single Diamond structure and the chiral single Gyroid structure. In many self-assembly processes the two corresponding double Gyroid and double Diamond structures compete for stability, with small differences in free energies and various systems where both forms occur, both synthetic and biological [71,73,75]. Why the single Gyroid is observed in the butterfly wing scales whereas the single Diamond is observed in beetle cuticles is an open and intriguing question. The answer may be provided by the physical chemistry of biological membranes, or by evolutionary biology, or by a combination of both – with the analysis of this article demonstrating that chiral optics is unlikely to play a role for this question. *Suivez ce papillon. Il ne sait pas où il va, c'est là que nous allons.*[11]

7. Materials & Methods

7.1. Specimens

Specimen of *Callophrys rubi*, *Teinopalpus imperialis*, *Canthon fulgidus* and *Plusiotis optima* were bought commercially from The Insect Collector (www.theinsectcollector.com).

7.2. Scanning electron microscopy (SEM)

Wing scales were investigated by SEM using a LEO GEMINI 1530 VP FEG-SEM electron microscope. Prior imaging and to prevent charging effects, the samples were sputter-coated with gold-palladium using an Emitech sputter coater.

7.3. Circular polarisation resolved spectrometry and absorption spectra

Reflectance spectra were measured with a custom-built microspectrophotometer, which consisted of a xenon light source, a Leitz Ortholux microscope and a fibre optic spectrometer (Avantes USB-2, Avantes, Eerbeek, The Netherlands). The microscope objective was an Olympus 20x/0.45 objective. To optimise UV-transmittance, most optics in the system were exchanged with quartz lenses. The reflectance was measured relative to a white reflectance standard (Spectralon, Labsphere, North Sutton, NH, USA). The circular polarisation measurements were performed by inserting a custom-built circular polarisation filter, consisting of a Thorlabs AQWP05M-340 achromatic quarter-wave plate and a HMPB linear polariser (Polaroid). The illuminated area was in the order of several tens of micrometers, while

[11] from Jean-Pol Vigneron's death notice, www.inmemoriam.be/fr/2013-06-24/jean-pol-vigneron/

the measured area was comparably small, approximately 6 µm × 6 µm for both beetle and the butterfly samples. The sample was illuminated from normal incidence with an opening polar angle of the light source of approximately 15°.

The absorbance spectra of the pigments in the wing scales were calculated from transmittance spectra obtained from single wing scales, immersed in a fluid with refractive index $n = 1.6$ (Cargille Labs, Cedar Grove, NJ, USA), and measured with a microspectrophotometer; an Olympus BX51 microscope with a 50x/0.8 Olympus objective, connected to an Ocean Optics QE6500 spectrometer (Ocean Optics Ltd, UK). The absorbance measurements were carried out in an area of size ≈ 20 µm × 20 µm.

7.4. Calculation of band diagrams by the frequency domain eigensolver method and their circular dichroism analysis

The band structure modes, i.e. the frequency eigenvalues $\Omega(\vec{k})$ and the corresponding magnetic eigenfields $\vec{H}_{\vec{k}}(\vec{r})$, are calculated with the open source package MPB [76], a frequency domain eigensolver developed at MIT. The CD index C and the coupling index β from which the point color and size is determined respectively are given by the definition taken from [35]

$$C^{\pm}_{\mathbf{k},n} \propto \left| \sum_{\mathbf{G}} \left(\mathbf{e}_x \pm i\mathbf{e}_y \right) \cdot \mathbf{h}_{\mathbf{G}} \int dx \int dy \, e^{i\mathbf{G}\cdot\mathbf{r}} \right|^2$$

$$C = \mathrm{sgn}(\mathbf{q} \cdot \nabla_k \omega) \frac{C^{+}_{\mathbf{k},n} - C^{-}_{\mathbf{k},n}}{C^{-}_{\mathbf{k},n} + C^{+}_{\mathbf{k},n}}$$

$$\beta = C^{+}_{\mathbf{k},n} + C^{-}_{\mathbf{k},n} \, .$$

7.5. FDTD method for simulations of Gyroid nanostructures with absorbing pigments

For time-domain simulations, the free finite-differences time-domain (FDTD) package MEEP [77] is used. Within the finite-differences approach, the governing differential equations (i. e. the real-space time-domain Maxwell equations) are discretised onto a regular lattice in time (equidistant time steps) and space (cubic voxels on the Yee grid [78]). Propagation of electromagnetic fields is simulated by timestep-wise forward integration.

For the irradiation, the source emits a pulse Gaussian-enveloped in frequency ($\sigma(\Omega) = 0.026$), of which several are assembled to broad-band reflectance spectra.

The object to be probed are defined by the spatial structure $\varepsilon(\vec{r})$ of its dielectric response. The choice of material per simulation grid point is made by the nodal approximation inequality eq. (1) between ambient ($\varepsilon = 1$) and Gyroid material.

Gyroid material and absorbance modelling. The Gyroid material is defined as a dielectric with static permittivity chosen to $\varepsilon_\infty = 2.4$. Absorbance is modeled as the (complex) dielectric response by the frequency-dependent permittivity of Lorentzian oscillators, as already explained in section 5.

The parameters of equation (3) are chosen that way that the simulated transmittance fits best to experimental data. This is shown in fig. 6 as a comparison of experimental absorbance data from *C. rubi* wingscales with simulated data, where in both cases the hollow Gyroid channel is filled with material of same $\mathrm{Re}(\varepsilon)$ as the dielectric channel (index matching, cf. section 5).

Layer thickness and variation. A layer of thickness $N_z \times a$ of the Gyroid structure defined by eq. (1) (including rotation) within the borders $z_\mathrm{T} < z < N_z \times a + z_\mathrm{T}$ in normal (z) direction; therefore the additional parameter z_T determines the termination phase, i. e. the particular plane perpendicular to the normal direction, which cuts through the Gyroid to become the surface. By varying over distinct z_T, effects of individual terminations are averaged out.

As visible from SEM images (fig. 1**C**), the Gyroid layer in the *C. rubi* wingscales exhibits a thickness of about 2 µm ≈ 6a. Thus, the layer thickness N_z of the FDTD simulation is chosen close to 6, in units of the structural length a. For [110] and [111] inclinations, this equals approx. 4.2 and 7.0 repetition units in normal direction, respectively.

In order to average over effects arising from distinct layer thickness, N_z is varied in steps of $0.2a$ from 5.5 to 6.1 times a. Lateral dimensions are chosen to fit proper continuation by periodic boundaries, while in normal direction, the light source and flux measurement is positioned in vacuum well apart the surfaces.

Acknowledgements

We dedicate this work to the memory of Jean-Pol Vigneron, to honour his legacy of scientific contributions to the field of structural color and biophotonics as much as his vital role in creating a vibrant interdisciplinary community.

We are endebted to Stephen Hyde and Doekele Stavenga for inspiration and ongoing support. We thank László Biró for his comment alerting us to the presence of pigments in the Gyroid wing scales of *C. rubi*. GEST is grateful for the hospitality of the Department of Applied Maths at the Australian National University, and to Mohan Srinivasarao for enlightening discussions and pointing our relevant literature references. We thank Philippe Lambin and Karin Derochette for the hospitality during the 'Living Light 2014' conference in Namur, Belgium.

References

[1] Michelson A. LXI. On metallic colouring in birds and insects. Philos Mag 1911. 21(124):554–567.
[2] Arwin H, Magnusson R, Landin J, Järrendahl K. Chirality-induced polarization effects in the cuticle of scarab beetles: 100 years after Michelson. Philos Mag 2012. 92(12):1583–1599.
[3] Sharma V, Crne M, Park J, Srinivasarao M. Bouligand structures underlie scarab beetle iridescence. Mater Today: Proc, in this issue 2014. TBA:TBA.
[4] Berthier S, Thomé M, Simonis P. Circular polarization in nature: factual, theoretical and experimental summary. Mater Today: Proc, in this issue 2014. TBA:TBA.
[5] Jewell SA, Vukusic P, Roberts NW. Circularly polarized colour reflection from helicoidal structures in the beetle plusiotis boucardi. New J Phys 2007. 9(4):99.
[6] Sharma V, Crne M, Park JO, Srinivasarao M. Structural origin of circularly polarized iridescence in jeweled beetles. Science 2009. 325:449–451.
[7] Mitov M. Cholesteric Liquid Crystals with a Broad Light Reflection Band. Adv Mater 2012. 24(47):6260–6276.
[8] Wynberg H, Meijer EW, Hummelen JC, Dekkers HPJM, Schippers PH, Carlson AD. Circular polarization observed in bioluminescence. Nature 1980. 286(5773):641–642. 10.1038/286641a0.
[9] Chiou TH, Kleinlogel S, Cronin T, Caldwell R, Loeffler B, Siddiqi A, Goldizen A, Marshall J. Circular polarization vision in a stomatopod crustacean. Curr Biol 2008. 18(6):429–434.
[10] Kleinlogel S, White AG. The secret world of shrimps: Polarisation vision at its best. PLoS ONE 2008. 3(5):e2190.
[11] Wilts BD, Whitney HM, Glover BJ, Steiner U, Vignolini S. Natural helicoidal structures: Morphology, self-assembly and optical properties. Mater Today: Proc, in this issue 2014. TBA:TBA.
[12] Vignolini S, Rudall PJ, Rowland AV, Reed A, Moyroud E, Faden RB, Baumberg JJ, Glover BJ, Steiner U. Pointillist structural color in pollia fruit. PNAS 2012. (pp. 15712–15715).
[13] Hyde ST, O'Keeffe M, Proserpio DM. A short history of an elusive yet ubiquitous structure in chemistry, materials and mathematics. Angew Chem Int Ed 2008. 47(42):7996–8000.
[14] Michielsen K, Stavenga DG. Gyroid cuticular structures in butterfly wing scales: biological photonic crystals. J R Soc Interface 2008. 5:85–94.
[15] Saranathan V, Osuji C, Mochrie S, Noh H, Narayanan S, Sandy A, Dufresne E, Prum R. Structure, function, and self-assembly of single network gyroid (I4132) photonic crystals in butterfly wing scales. PNAS 2010. 107:11676–11681.
[16] Schröder-Turk G, Wickham S, Averdunk H, Large M, Poladian L, Brink F, Fitz Gerald J, Hyde ST. The chiral structure of porous chitin within the wing-scales of callophrys rubi. J Struct Biol 2011. 174:290–295.
[17] Mille C, Tyrode EC, Corkery RW. Inorganic chiral 3-d photonic crystals with bicontinuous gyroid structure replicated from butterfly wing scales. Chem Commun 2011. 47:9873–9875.
[18] Mille C, Tyrode EC, Corkery RW. 3D titania photonic crystals replicated from gyroid structures in butterfly wing scales: approaching full band gaps at visible wavelengths. RSC Adv 2013. 3:3109–3117.
[19] Wilts B, Stavenga ID. Pigmentary and photonic coloration mechanisms reveal taxonomic relationships of the cattlehearts (lepidoptera: Papilionidae : Parides). BMC Evol Biol 2014. in press.
[20] Yoshioka S, Fujita H, Kinoshita S, Matsuhana B. Alignment of crystal orientations of the multi-domain photonic crystals in parides sesostris wing scales. J R Soc Interface 2014. 11(92):20131029.
[21] Argyros A, Manos S, Cox G, Dwarte D, Large M. Electron tomography and computer visualisation of a 3-dimensional "photonic" crystal in a butterfly wing-scale. Micron 2002. 33(5):483–487.
[22] Wilts BD, Michielsen K, Kuipers J, De Raedt H, Stavenga DG. Brilliant camouflage: photonic crystals in the diamond weevil, entimus imperialis. Proc R Soc B 2012. (pp. 2524–2530).
[23] Kertész K, Bálint Z, Vértesy Z, Márk GI, Lousse V, Vigneron JP, Rassart M, Biró LP. Gleaming and dull surface textures from photonic-crystal-type nanostructures in the butterfly cyanophrys remus. Phys Rev E 2006. 74:021922.
[24] Michielsen K, De Raedt H, Stavenga DG. Reflectivity of the gyroid biophotonic crystals in the ventral wing scales of the green hairstreak butterfly, callophrys rubi. J R Soc Interface 2010. 7(46):765–771.
[25] Poladian L, Wickham S, Lee K, Large MC. Iridescence from photonic crystals and its suppression in butterfly scales. J R Soc Interface 2009. 6(2047):S233–S242.

[26] Wilts BD, Michielsen K, De Raedt H, Stavenga DG. Iridescence and spectral filtering of the gyroid-type photonic crystals in parides sesostris wing scales. Interface Focus 2011. 2(5):681–687.
[27] Turner MD, Schröder-Turk GE, Gu M. Fabrication and characterization of three-dimensional biomimetic chiral composites. Opt Express 2011. 19(10):10001–10008.
[28] Turner MD, Saba M, Zhang Q, Cumming BP, Schröder-Turk GE, Gu M. Miniature chiral beamsplitter based on gyroid photonic crystals. Nature Photon 2013. 7(10):801–805.
[29] Cumming BP, Turner MD, Schröder-Turk GE, Debbarma S, Luther-Davies B, Gu M. Adaptive optics enhanced direct laser writing of high refractive index gyroid photonic crystals in chalcogenide glass. Opt Express 2014. 22(1):689–698.
[30] Schoen AH. Infinite periodic minimal surfaces without self-intersections. Technical Note TN D-5541, NASA, 1970.
[31] Heesch H, Laves F. Über dünne Kugelpackungen. Z Krist 1933. 85(1):443–453.
[32] Schoen AH. Reflections concerning triply-periodic minimal surfaces. Interface Focus 2012. 85:346–362.
[33] Delgado-Friedrichs O, O'Keeffe M, Yaghi O. Three-periodic nets and tilings: regular and quasiregular nets. Acta Cryst 2003. A59:22–27.
[34] Grosse-Braukmann K. On Gyroid interfaces. J Colloid Interface Sci 1997. 187:418–428.
[35] Saba M, Thiel M, Turner M, Hyde ST, Gu M, Grosse-Brauckmann K, Neshev D, Mecke K, Schröder-Turk GE. Circular dichroism in biomimetic cubic chiral nets. Phys Rev Lett 2011. 106:103902.
[36] Michielsen K, Kole JS. Photonic band gaps in materials with triply periodic surfaces and related tubular structures. Phys Rev B 2003. 68:115107.
[37] Vignolini S, Yufa NA, Cunha PS, Guldin S, Rushkin I, Stefik M, Hur K, Wiesner U, Baumberg JJ, Steiner U. A 3d optical metamaterial made by self-assembly. Adv Mater 2011. (pp. OP23–OP27).
[38] Hur K, Francescato Y, Giannini V, Maier SA, Hennig RG, Wiesner U. Three-dimensionally isotropic negative refractive index materials from block copolymer self-assembled chiral gyroid networks. Angew Chem Int Ed 2011. (pp. 11985–11989).
[39] Oh SS, Demetriadou A, Wuestner S, Hess O. On the origin of chirality in nanoplasmonic gyroid metamaterials. Adv Mater 2012. (pp. 612–617).
[40] Almsherqi Z, Margadant F, Deng Y. A look through 'lens' cubic mitochondria. Interface Focus 2012. 2(5):539–545.
[41] Maldovan M, Urbas AM, Yufa N, Carter WC, Thomas EL. Photonic properties of bicontinuous cubic microphases. Phys Rev B 2002. 65:165123.
[42] Lu L, Fu L, Joannopoulos JD, Soljačić M. Weyl points and line nodes in gyroid photonic crystals. Nature Photon 2013. 7(4):294–299.
[43] Pouya C, Vukusic P. Electromagnetic characterization of millimetre-scale replicas of the gyroid photonic crystal found in the butterfly parides sesostris. Interface Focus 2012. 2(5):645–650.
[44] Hecht E. Optics. Addison-Wesley, 1998.
[45] Sihvola AH. Electromagnetic modeling of bi-isotropic media. PIER 1994. 9:45–86.
[46] Guerin F. Energy dissipation and absorption in reciprocal bi-isotropic media described by different formalisms. PIER 1994. 9:31–44.
[47] Saba M, Turner MD, Mecke K, Gu M, Schröder-Turk GE. Group theory of circular-polarization effects in chiral photonic crystals with four-fold rotation axes applied to the eight-fold intergrowth of gyroid nets. Phys Rev B 2013. (88):245116.
[48] Arwin H, Berlind T, Johs B, Järrendahl K. Cuticle structure of the scarab beetle cetonia aurata analyzed by regression analysis of mueller-matrix ellipsometric data. Opt Express 2013. 21(19):22645–22656.
[49] Arwin H, Magnusson R, Fernanández del Río L, Åkerlind C, Muñoz-Pineda E, Landin J, Mendoza-Galvan A, Järrendahl K. Exploring optics of beetle cuticles with Mueller-matrix ellipsometry. Mater Today: Proc, in this issue 2014. TBA:TBA.
[50] Neville AC, Caveney S. Scarabaeid beetle exocuticle as an optical analogue of cholesteric liquid crystals. Biological Reviews 1969. 44:531–562.
[51] Neville A. Metallic gold and silver colours in some insect cuticles. J Insect Physiol 1977. 23(10):1267–1274.
[52] Ashcroft NW. Solid state physics. 2006. 09GP80/21.2.1 A823+2.
[53] Yoshioka S, Matsuhana B, Fujita H. Polarization-dependent tessellated pattern of the wing scale of *parides sesostris* butterfly. Mater Today: Proc, in this issue 2014. TBA:TBA.
[54] Saba M, Schröder-Turk G. Complex bandstructures for complex geometries. Crystals 2014. in preparation.
[55] McGraw KJ. The antioxidant function of many animal pigments: are there consistent health benefits of sexually selected colourants? Anim Behav 2005. 69(4):757–764.
[56] Umebachi Y. Papiliochrome, a new pigment group of butterfly. Zoolog Sci 1985. 2(2):163–174.
[57] Stavenga DG, Giraldo MA, Leertouwer HL. Butterfly wing colors: glass scales of graphium sarpedon cause polarized iridescence and enhance blue/green pigment coloration of the wing membrane. J Exp Biol 2010. 213(10):1731–1739.
[58] Wijnen B, Leertouwer HL, Stavenga DG. Colors and pterin pigmentation of pierid butterfly wings. J Insect Physiol 2007. 53(12):1206–1217.
[59] Reed RD, Nagy LM. Evolutionary redeployment of a biosynthetic module: expression of eye pigment genes vermilion, cinnabar, and white in butterfly wing development. Evol Devel 2005. 7(4):301–311.
[60] Rutowski R, Macedonia J, Morehouse N, Taylor-Taft L. Pterin pigments amplify iridescent ultraviolet signal in males of the orange sulphur butterfly, colias eurytheme. Proc R Soc B 2005. 272(1578):2329–2335.
[61] Wilts BD, Trzeciak TM, Vukusic P, Stavenga DG. Papiliochrome ii pigment reduces the angle dependency of structural wing colouration in nireus group papilionids. J Exp Biol 2012. 215(5):796–805.
[62] Stavenga DG, Tinbergen J, Leertouwer HL, Wilts BD. Kingfisher feathers–colouration by pigments, spongy nanostructures and thin films. J Exp Biol 2011. 214(23):3960–3967.
[63] D'Alba L, Kieffer L, Shawkey MD. Relative contributions of pigments and biophotonic nanostructures to natural color production: a case study in budgerigar (melopsittacus undulatus) feathers. J Exp Biol 2012. 215(8):1272–1277.
[64] Stavenga DG, Leertouwer HL, Hariyama T, De Raedt HA, Wilts BD. Sexual dichromatism of the damselfly *Calopteryx japonica* caused by a

melanin-chitin multilayer in the male wing veins. PLoS ONE 2012. 7(11):e49743.
[65] Leertouwer HL, Wilts BD, Stavenga DG. Refractive index and dispersion of butterfly chitin and bird keratin measured by polarizing interference microscopy. Opt Express 2011. 19(24):24061–24066.
[66] Salvatore S, Demetriadou A, Vignolini S, Oh SS, Wuestner S, Yufa NA, Stefik M, Wiesner U, Baumberg JJ, Hess O, *et al.* Tunable 3d extended self-assembled gold metamaterials with enhanced light transmission. Adv Mater 2013. 25(19):2713–2716.
[67] Galusha JW, Richey LR, Gardner JS, Cha JN, Bartl MH. Discovery of a diamond-based photonic crystal structure in beetle scales. Phys Rev E 2008. 77(5):050904.
[68] Pouya C, Stavenga DG, Vukusic P. Discovery of ordered and quasi-ordered photonic crystal structures in the scales of the beetle eupholus magnificus. Opt Express 2011. 19(12):11355–11364.
[69] Pouya C. Investigating Naturally Occurring 3-Dimensional Photonic Crystals. Phd thesis, University of Exeter, 2012.
[70] Ghiradella H. Structure and development of iridescent lepidopteran scales: The papilionidae as a showcase family. Ann Entomol Soc Am 1985. 2(78):252–264.
[71] Hyde ST, Schröder-Turk GE. Geometry of interfaces: topological complexity in biology and materials. Interface Focus 2012. 2(5):529–538.
[72] Almsherqi ZA, Landh T, Kohlwein SD, Deng YR. Cubic membranes: The missing dimension of cell membrane organization. Int Rev Cell Mol Biol 2009. 274:275–342.
[73] Almsherqi Z, Kohlwein S, Deng Y. Cubic membranes: a legend beyond the flatland* of cell membrane organization. J Cell Biol 2006. 173(6):839–844.
[74] Schröder-Turk GE, Fogden A, Hyde ST. Bicontinuous geometries and molecular self-assembly: Comparison of local curvature and global packing variations in genus-three cubic, tetragonal and rhombohedral surfaces. Eur Phys J B 2006. 54:509–524.
[75] Hyde ST, Andersson S, Larsson K, Blum Z, Landh T, Lidin S, Ninham B. The Language of Shape. Elsevier Science, Amsterdam, 1st edition, 1997.
[76] Johnson SG, Joannopoulos JD. Block-iterative frequency-domain methods for maxwell's equations in a planewave basis. Opt Express 2001. 8(3):173–190.
[77] Oskooi AF, Roundy D, Ibanescu M, Bermel P, Joannopoulos J, Johnson SG. Meep: A flexible free-software package for electromagnetic simulations by the FDTD method. Comput Phys Commun 2010. 181(3):687–702.
[78] Yee KS. Numerical solution of initial boundary value problems involving maxwells equations in isotropic media. IEEE Trans Antennas Propagat 1966. 14(3):302–307.